1-1-2019

Predicting neural recording performance of implantable electrodes

Alexander R. Harris
University of Wollongong, alexh@uow.edu.au

Ben Allitt
Chisholm Institute

Antonio G. Paolini
La Trobe University, a.paolini@latrobe.edu.au

Predicting neural recording performance of implantable electrodes

Abstract

Recordings of neural activity can be used to aid communication, control prosthetic devices or alleviatedisease symptoms. Chronic recordings require a high signal-to-noise ratio that is stable for years. Currentcortical devices generally fail within months to years after implantation. Development of novel devices toincrease lifetime requires valid testing protocols and a knowledge of the critical parameters controllingelectrophysiological performance. Here we present electrochemical and electrophysiological protocolsfor assessing implantable electrodes. Biological noise from neural recording has significant impact on signal-to-noise ratio. A recently developed surgical approach was utilised to reduce biological noise. This allowed correlation of electrochemical and electrophysiological behaviour. The impedance versus frequency of modified electrodes was non-linear. It was found that impedance at low frequencies was astronger predictor of electrophysiological performance than the typically reported impedance at 1 kHz.Low frequency impedance is a function of electrode area, and a strong correlation of electrode area with electrophysiological response was also seen. Use of these standardised testing protocols will allow future devices to be compared before transfer to preclinical and clinical trials.

Disciplines

Engineering | Physical Sciences and Mathematics

Publication Details

Harris, A. R., Allitt, B. J. & Paolini, A. G. (2019). Predicting neural recording performance of implantable electrodes. Analyst, 144 (9), 2973-2983.

Predicting Neural Recording Performance of Implantable Electrodes

Alexander R. Harris[1], Ben J. Allitt[2], Antonio G. Paolini[3,4]

[1] ARC Centre of Excellence for Electromaterials Science, Intelligent Polymer Research Institute, University of Wollongong, NSW 2522, Australia.
[2] Health and Community Care, Chisholm Institute, Dandenong, Victoria, 3175, Australia
[3] ISN Psychology, Institute for Social Neuroscience, 6/10 Martin St, Heidelberg, Victoria 3084, Australia
[4] School of Psychology and Public Health, La Trobe University, Bundoora, Victoria, 3086, Australia

Email: alexrharris@gmail.com

Abstract

Recordings of neural activity can be used to aid communication, control prosthetic devices or alleviate disease symptoms. Chronic recordings require a high signal-to-noise ratio that is stable for years. Current cortical devices generally fail within months to years after implantation. Development of novel devices to increase lifetime requires valid testing protocols and a knowledge of the critical parameters controlling electrophysiological performance. Here we present electrochemical and electrophysiological protocols for assessing implantable electrodes. Biological noise from neural recording has significant impact on signal-to-noise ratio. A recently developed surgical approach was utilised to reduce biological noise. This allowed correlation of electrochemical and electrophysiological behaviour. The impedance versus frequency of modified electrodes was non-linear. It was found that impedance at low frequencies was a stronger predictor of electrophysiological performance than the typically reported impedance at 1 kHz. Low frequency impedance is a function of electrode area, and a strong correlation of electrode area with electrophysiological response was also seen. Use of these standardised testing protocols will allow future devices to be compared before transfer to preclinical and clinical trials.

Introduction

Neurons are excitable cells, able to generate and detect electrical current. When a neuron fires an action potential, ion channels in the cell membrane open. Movement of ions across the membrane change the local potential according to the Goldman equation (1). The resting potential across a neuronal membrane is approximately -70 mV, and during an action potential it can rise to over 100 mV. This change in potential can be measured via patch clamping, where an electrolyte filled glass pipette is placed on or inserted into the cell and a reference-ground electrode is placed in solution outside the cell, forming an electrical circuit (2). While patch clamping allows highly sensitive measurements from a

single cell, *in vivo* recordings must be made within a complex neural structure composed of multiple cell types. The large size and fragile nature of the glass pipettes limits their utility in chronic *in vivo* studies. Furthermore, piercing the cell membrane leads to cell death, so chronic *in vivo* electrophysiological recordings are obtained external to the cell wall.

The Michigan and Utah style microelectrode arrays (MEAs) are microfabricated silicon structures with metal electrodes (3) (4). Over 1000 individually addressable electrodes have been incorporated into 3 dimensional MEAs (5). MEAs allow parallel recordings and redundancy to ensure target neurons are in close proximity to an electrode. The designs minimise the electrode impedance and interelectrode coupling to limit background noise (6). Implanted electrodes can be used to detect neural activity associated with epileptic seizures and improve management procedures like triggering electrical stimulation to cease the seizure (7). Neural recordings from the motor cortex can also be used to enable communication or control prosthetic devices for people suffering from motor neurone disease or trauma (8).

Insertion of an electrode array into the brain is highly invasive, inducing neural death and micro-haemorrhages. After implantation, neural rearrangement and a foreign body response can occur, where the electrode array is typically surrounded by a glial cell sheath (9). As a result, recorded activity varies day-to-day and an initial high amplitude neural recording can degrade over time (10). Different strategies have been used to reduce the foreign body response. The electrode arrays are typically tethered to the skull, however movement due to body motion, respiration and blood circulation can induce further microtraumas (11). Untethered electrode arrays have shown reduced foreign body response (12). The rigid silicon arrays have a Young's modulus in the 200 GPa range, significantly higher than neural tissue of ~1 kPa (13). Use of flexible polymer substrates, such as polyimide, and soft coatings like hydrogels allow the electrode array to move and conform to the brain structure. However these materials are still harder than neural tissue, and insertion of these flexible materials without deformation is difficult. To aid insertion, a rigid shuttle or dissolvable carrier can be attached to the flexible array, although the larger probe size with the shuttle can increase surgical trauma. Drug elution from the probe can be used to improve device performance, with anti-inflammatories such as dexamethasone reducing inflammation associated with surgical trauma and nerve growth factors inducing neural growth towards the electrode (14).

Even with a device that shows minimal foreign body response, there is still a need to increase the signal-to-noise ratio of neural recordings. Clinical implants use platinum electrodes, as they are corrosion resistant and non-cytotoxic. Modification of the electrode surface has been used as a method for controlling neural growth and reducing the electrode impedance. Electrode modifications include nanostructuring the platinum (15), deposition of doped conducting polymers (16) and use of other conducting materials such as iridium oxide (17) or graphene (18).

With an increasing number of electrode materials and designs being proposed, valid *in vitro* and *in vivo* testing protocols must be used to compare device performance before they are used in expensive preclinical and clinical trials (19) (20). In addition, a greater theoretical understanding of charge transfer across the electrode-tissue interface is required. Electrochemical impedance spectroscopy (EIS) is typically measured to assess an electrodes thermal noise and signal-to-noise ratio. EIS applies an AC voltage waveform at different applied frequencies to an electrode, measuring the current. A small voltage amplitude is used to ensure a near linear response between voltage and current. It is generally assumed that an action potential has a characteristic frequency of 1 kHz, and so the EIS should be measured at this frequency. However an action potential contains information from 0 Hz to over 3 kHz (21), there is no characteristic frequency. More importantly, the measurement performance of the electrode depends on the electrode-solution interfacial impedance and not the Fourier spectrum of the action potential. This interfacial impedance is often a non-linear function with applied frequency, and so assessment of electrode function at 1 kHz may not be optimal for predicting electrophysiological performance. This article compares the electrochemical and electrophysiological response of bare metal and doped conducting polymer modified electrodes to determine the key electrode properties that control neural recording sensitivity. A recently developed acute surgical protocol is utilised to reduce biological noise for device comparison (22) (23). Strong correlations of electrophysiological response with impedance at 12 Hz and electrode area indicate *in vitro* testing protocols should include impedance at low frequencies instead of the more common 1 kHz measurement.

Methods

Materials and Electrode Coating

3,4-ethylenedioxythiophene (EDOT), poly(styrenesulfonate) (PSS, MW = 70,000), sodium dodecylbenzenesulfonate (NaDBSA), sodium *para*-toluene sulfonate (Na_2pTs), hexaammineruthenium(III) chloride ($Ru(NH_3)_6\ Cl_3$) (Sigma-Aldrich) and 99.0 % di-sodium phosphate (Fluka) were used as received. Polymer coatings were deposited on 4 shank, 32 electrode (8 electrodes per shank), 413 μm^2 nominal geometric area platinum electrodes with 200 μm pitch (Neuronexus Technologies – A4x8-5mm-200-200-413). Conducting polymer coatings with different dopants were electrochemically deposited onto individual microelectrodes via a potentiostat (CH660D, CH Instruments) from mixed solutions containing 10 mM EDOT and 0.1 M Na_2pTs or 2 mg mL^{-1} NaDBSA or PSS in deionised water. Potentiostatic growth was performed in a three-electrode configuration using one microelectrode as the working electrode, Ag/AgCl (3 M NaCl) as reference electrode and Pt mesh as counter electrode. Solutions were degassed for 30 minutes with nitrogen before depositing the electrode coatings. All polymers were deposited at 1 V vs Ag/AgCl. PEDOT-PSS and PEDOT-DBSA were deposited for 4 different times (15, 30, 45 or 60 s), PEDOT-pTs was deposited for 45s as recommended in our previous article (22). 1 probe was coated with PEDOT-PSS and 1 with PEDOT-

DBSA, 4 electrode sites coated at each deposition time in a staggered array as previously described (22), leaving 12 uncoated platinum electrodes and 4 PEDOT-pTs coated electrodes as controls.

Electrodes were imaged using a BX61 optical microscope (Olympus) and the geometric area measured with ImageJ (figure 1a). Electrochemical analysis was undertaken in 0.3 M phosphate buffer in deionised water and the electroactive areas measured by addition of 5 mM $Ru(NH_3)_6^{3+}$. Test solutions were not degassed. A CHI660B potentiostat with CHI684 multiplexer (CH Instruments) were used to perform cyclic voltammetry at each of the individually addressable working electrode sites. A 3 electrode configuration was used with a Ag/AgCl (3 M KCl) reference and Pt mesh counter electrode. Charge density measurements were performed using cyclic voltammetry over a range of 0.8 to -0.8 V vs Ag/AgCl at a scan rate of 100 mV s^{-1}. Electroactive area measurements were undertaken over a range of 0 to -0.5 V varying the scan rate from 10 mV s^{-1} to 1 V s^{-1}. EIS was performed at 0 V with a 10 mV amplitude over a frequency range of 10-100,000 Hz to compare with previous data on conducting polymer modified neural electrodes. Equivalent circuit fitting of the EIS data was performed with ZView.

In vivo Testing

Experimental procedures were performed in a sound attenuating Faraday cage on an anti-vibration table. Hooded Wistar rats weighing over 200 g were anesthetised with urethane (20% v/v in distilled water, 1.3 g/kg i.p., Sigma-Aldrich). The animal was placed in a stereotaxic frame (David Kopf Instruments) fitted with a hollow ear bar in the left ear. Animal temperature was monitored continuously via a rectal probe and maintained at 37.5 °C using an ATC1000 DC temperature controller (World Precision Instruments). A craniectomy was performed to access the right inferior colliculus (IC). A Ag/AgCl wire reference electrode wrapped in saline saturated cotton wool was placed into the dorsal region of the animals neck. The multichannel polymer electrode was then inserted at a 19° rostro-caudal angle with reference to Lambda using stereotaxic coordinates and a rat brain atlas (24) approximately 2 mm into the brain, towards the IC. White noise bursts were generated by a RX6 multifunction processor and PA5 programmable attenuator (Tucker-Davis Technologies) controlled by custom software developed in OpenEx. Sound was delivered through the left ear bar using an EC1 electrostatic speaker driven using an ED1 electrostatic speaker driver (Tucker-Davis Technologies). Prior to use, the speaker was calibrated by attachment of the sound generation system to one end of the ear bar with a one-eighth-inch 4138-A-015 microphone and amplifier unit and 2829 4-Channel Microphone Power Supply (Brüel and Kjær) coupled to the other end using a 3 mm long rigid plastic tube to mimic the rat's ear canal. The electrode was then advanced into the IC using a motorized microdrive (Sutter Instruments), whilst monitoring the neural response via a PZ2 high impedance amplifier and RZ2 bioamp processor (Tucker-Davis Technologies) with band-pass filtering (300–5000 Hz), until roughly the bottom 3 electrodes on each shank displayed acoustically driven activity.

An acoustic stimulation protocol of 300 repetitions of 50 ms white noise bursts (rise-fall time 10 ms, Gaussian distributed noise, 1–44 kHz) at a 1 s repetition rate was then delivered through the speaker at 70 dB, while recording the multiunit activity at each electrode (acquired at a sampling rate of 24.4 kHz). On completion of the acoustic stimulation protocol, the probe was advanced ~200 μm into the IC so that each electrode was in approximately the same position as the more distal electrode from the first measurement. The acoustic stimulation was then repeated and the probe advanced in 200 μm steps until all of the electrodes had recorded acoustically evoked activity. The probe was then retracted in 200 μm steps using the same acoustic stimulation protocol to determine the reproducibility of the measurements and potential damage caused from the probe insertion. After *in vivo* recording, the electrodes were carefully retracted from the animal and gently rinsed with deionised water before storing. All animal procedures were in accordance with the "Australian code for the care and use of animals for scientific purposes" and approved by the RMIT University Animal Ethics Committee (AEC Number 1315) published previously (23).

Data Analysis

Acoustically evoked responses were imported into Matlab for offline analysis. A Fourier transform of the complete 300 s noise pulse train was performed. A bandpass filter of 300-5000 Hz was applied for measuring multi-unit activity and a bandpass filter of 60-300 Hz was applied for assessing local field potentials (LFP). For each electrode site, the average of the bandpass filtered RMS measured during acoustic stimulation (RMS_{stim}) for the complete 50 ms stimulation period was averaged from the 300 repetitions at one electrode depth. The average of the bandpass filtered RMS outside the acoustic stimulation period (RMS_{bkgd}) was only performed over the last 300 ms of the 950 ms time and averaged from the 300 repetitions at one electrode depth, to eliminate artifacts from neuron refractory periods. The signal to noise ratio (SNR) was calculated from (RMS_{stim} / RMS_{bkgd}) with the SNR classification taken from (25) (where low SNR < 3.5, medium SNR 3.5-4.0 and good SNR > 4.0). A spike was measured where the recorded potential was >4.2 x S.D. of the RMS from the previous 1 s with an exponential weighting of signal for recency. The "during" and "outside" acoustic stimulation spike count was then performed over the same time periods as above. The spike count difference was calculated from (spike count during stimulation) – (spike count outside stimulation). Each electrode site was considered "in" the IC when the spike count difference at one electrode depth was greater than 45 % of the maximum recorded spike count difference over the whole experiment. Data for each electrode site was averaged across all electrode depths "in" the IC to reduce error due to variations in biological noise (the number of recordable neurons in the vicinity of the electrodes).

Results

Microscopy and Electrochemistry

Microelectrodes were coated with doped conducting polymers at different deposition times (Figure 1a). The conducting polymers grew out from the electrode surface, increasing in geometric area with deposition time and charge passed during electrodeposition (26). The electrodeposited PEDOT-PSS and PEDOT-DBSA displayed a nodular, rough structure while the PEDOT-pTs deposited for 45 s was more uniform. At longer deposition times, the conducting polymer grew to the edge of the silicon shank. This was more pronounced at the shank tips, where the shank width was smaller. With a 45 s deposition time, PEDOT-PSS and PEDOT-DBSA were double the geometric area of PEDOT-pTs (26) which is most likely due to polymer templating by the different dopant ions during electrodeposition (27). The geometric area of the electrodes was assessed by visible light microscopy and seen to increase with deposition time and deposition charge (26). Deviations from this response were seen when the conducting polymer grew to the edge of the shank.

Cyclic voltammetry is typically used to assess an electrode's charge injection capacity and charge density. The safe charge injection capacity of an electrode should only include potential regions that do not generate toxic species. Therefore the potential range was chosen to be within the water oxidation and reduction window and carried out over a range of 0.8 to -0.8 V vs Ag/AgCl. The charge injection capacity is usually measured from the reduction sweep of the voltammogram. However recent studies have shown this is only valid for ideal electrodes, in practise the oxidation and reduction charge injection capacity are not equivalent (28). Platinum electrodes display a small current due to capacitance and some Faradaic current associated with oxygen reduction, oxide formation and removal, and hydride adsorption and stripping (Figure 1b). PEDOT modified electrodes have a significantly larger charge injection capacity including capacitance and Faradaic current from redox reactions of the conducting polymer. The charge injection capacity of the modified electrodes correlated with the deposition time and deposition charge, but deviated from this trend when the polymer contacted the edge of the shank (26).

Uncoated metal electrodes displayed an inverse response of impedance versus frequency (Figure 1c) and close to -90º phase angle typical of a capacitor (Figure 1d). Conducting polymer coated electrodes had increasing impedance with decreasing frequency, but with a plateau region at intermediate frequencies (29). The phase angle of coated electrodes was close to -90º at 100 kHz, approached 0º at intermediate frequencies around 1 kHz and then shifted more negative at low frequencies. The impedance of the electrodes could be fit with an equivalent circuit. The uncoated electrodes could be fit with a simple RC circuit while the modified electrodes required more complex equivalent circuits (29).

The effective electroactive area was assessed by addition of $Ru(NH_3)_6^{3+}$ to the test solution. Reduction of the $Ru(NH_3)_6^{3+}$ at fast voltammetric scan rates produced peak shaped voltammograms indicative of a linear diffusion profile of $Ru(NH_3)_6^{3+}$ to the electrode surface (Figure 2a). Measurement of the peak heights (i_p) can be used to calculate a linear diffusion effective area (A) according to

$$i_p = (2.69 \times 10^5) n^{3/2} A D^{1/2} c \upsilon^{1/2} \quad (1)$$

where n is the number of electrons transferred, D is the diffusion coefficient (9.0×10^{-6} cm^2 s^{-1}) (30), c is the concentration and υ is the scan rate. At slow voltammetric scan rates, diffusion of the $Ru(NH_3)_6^{3+}$ to the microelectrode obtains a radial profile. This results in a sigmoidal shaped voltammetric response (Figure 2b). The limiting current (i_{ss}) at a disc electrode has the form

$$i_{ss} = 4nFDcr \quad (2)$$

where F is the Faraday constant and r is the electrode radius. A steady-state current was obtained on all uncoated, PEDOT-DBSA and PEDOT-pTs electrodes, but not on PEDOT-PSS, as the electrodes were too large to achieve a radial diffusion profile at a voltammetric scan rate of 10 mV s^{-1}. The linear diffusion effective area was significantly larger than the geometric area due to high surface roughness (26). However the radial diffusion effective area was smaller than the geometric area indicating the radial diffusion profile was not uniform across the entire electrode surface (the electrode is not a perfect flat disc geometry) (31).

Electrophysiology

The microelectrode arrays were inserted into the inferior colliculus (IC) of a rat with white noise pulses presented to the ear. Multiunit activity was detected on each electrode in the IC, with an increase in RMS clearly visible during acoustic stimulation (Figure 3a) The average RMS outside of the acoustic stimulation was around 10-20 μV, depending on electrode coating (Table 1). A Fourier spectrum of the 300 noise pulse stream showed most power around 0 Hz, decreasing in magnitude to 5 kHz; no peaks in the Fourier spectrum were found (Figure 3b). Multiunit activity was assessed after applying a bandpass filter of 300-5000 Hz while local field potentials were assessed with a bandpass filter of 60-300 Hz.

When the electrodes were placed into the IC, activity was detected on the most distal electrodes; electrodes more proximal displayed no activity. Stepping the electrode array further into the IC resulted in more electrodes detecting activity. The spike count difference was found to be the most sensitive in detecting activity and used to define when each electrode was in the IC. Despite stimulating the IC with white noise, the local potential within the IC is not uniform. There was a variation in electrophysiological response within the IC due to biological noise (variation in electrode-neuron distance, number of neurons adjacent the electrode, local micro-haemorrhages etc.) (Figure 3c-d). The maximum SNR for most coated electrodes was deemed good (Table 1), however the maximum SNR

for each electrode was obtained from different positions in the IC. And there is an uncertainty in knowing if this is the absolute maximum SNR achievable with each electrode. To reduce the effect of biological noise, the electrophysiological responses were averaged over all the positions the electrode was deemed in the IC. While using an average electrophysiological response reduces biological noise, it also reduces the SNR; as a result, most average SNR values fell into the low-medium range (Table 1).

Electrode impedance is normally measured to assess its thermal noise and SNR. The impedance was plotted versus RMS_{bkgd}, SNR and mean during stimulation spike count (Figure 4). There was a weak positive correlation using a power curve between impedance at 1 kHz and RMS_{bkgd} and a moderate to strong negative correlation with SNR and mean during stimulation spike count.

The impedance of modified electrodes varies in a non-linear manner with frequency. Subsequently, an *in vitro* assessment of electrode performance at 1 kHz may not be optimal. Plots of RMS_{bkgd}, SNR and mean during stimulation spike count versus impedance at 12 Hz displayed a larger or equivalent correlation strength compared to impedance at 1 kHz (Figure 5). Plots of phase angle at 12 Hz versus SNR and mean during stimulation spike count had moderate to strong linear correlations with PEDOT-DBSA but were much weaker with PEDOT-PSS (Figure S1).

Changing the measured impedance frequency from 1 kHz to 12 Hz affected the correlation strength with electrophysiological performance. The impedance at low frequencies is dependent on electrode area (29). Therefore, the dependence of electrophysiological response with electrode area was assessed. The electrode area can be measured by different methods; optical microscopy provides a geometric area, while the effective electrochemically active area can be measured by reduction of $Ru(NH_3)_6^{3+}$ at fast or slow voltammetric scan rates. Each method provides different information on the electrode surface which may better predict electrophysiological performance. Correlations were made with a trendline of the form $Z = \frac{a}{A^2} + \frac{b}{A} + c$. Weak negative correlations were seen with geometric area, steady state diffusion electroactive area and linear diffusion electroactive area with RMS_{bkgd} (Figures S2-4). Moderate to strong positive correlations were seen with all PEDOT-DBSA electrode area measures versus SNR and mean during stimulation spike count. The best predictor of electrophysiological performance was seen with a steady state diffusion electroactive area and mean during stimulation spike count (Figure S3c). Electroactive area measurements from PEDOT-PSS were more variable with no steady state diffusion electroactive area obtained, and the linear diffusion electroactive area showing no correlation with geometric area, deposition time or deposition charge (26). This resulted in weak correlations of PEDOT-PSS linear diffusion electroactive area with electrophysiological response, while moderate correlations could be obtained with the geometric area.

The relationship of local field potential with electrode properties is also unknown. The LFP RMS_{bkgd} was 2-4 times larger than the multiunit activity RMS_{bkgd} and the LFP SNR was smaller. When stepping the electrode array through the IC, the SNR varies with position. The standard deviation in SNR from all electrode positions in the IC is related to the amount of biological noise. The standard deviation from multiunit activity and LFP for each deposition time of PEDOT-PSS was averaged (Table S1). The standard deviation in LFP was smaller than multiunit activity, indicating less biological noise for the LFP recordings. Similar to multiunit activity RMS_{bkgd}, the LFP RMS_{bkgd} had positive correlations with impedance at 1 kHz and 12 Hz, and negative correlations with phase angle at 12 Hz and electrode area (Figures 6-7, S5-8). The correlations with SNR were the opposite direction to the RMS_{bkgd}. In nearly every case, the correlation strength was equivalent or higher for the LFP than the multiunit activity.

Discussion

The use of implantable electrodes to record neural activity requires a stable and high SNR. Current clinical devices fail for a variety of reasons within a few months or years after implantation (32). While significant effort has been spent modifying device geometries and materials to improve biocompatibility and biostability, to date this work has not translated into new clinical applications. Typically new materials or devices are assessed by measuring impedance at 1 kHz, an ability to support cell growth in culture and measurement of electrophysiological activity from a microelectrode array or *in vivo* model. While device size, hardness, flexibility and material properties play a role in its biocompatibility, there is no consensus on what properties should be measured and reported. This prevents a comparison of novel devices and rational development of new clinical implants.

An electrophysiological technique is required to assess neural recording efficacy. This method should provide a background noise level and response to neural activity. This work measured electrophysiological behaviour in the IC of a rat which is easily accessible surgically. Reproducible neural activity is also easily elicited through delivery of multiple noise pulses to the ear. Spike count gave a larger response than RMS or SNR and was a better measure of correct placement of the electrode array in the IC. With an electrode in a fixed position, a single measure of electrophysiological response was obtained. There is a large uncertainty in this single measurement as it provides no information on the level of biological noise present. Electrophysiological recordings from multiple positions must be obtained to account for biological noise. A maximum or average response may then be reported. Control electrodes must also be included in each test, as the level of neural activity varies between individual animals.

Electrophysiological performance can be predicted from *in vitro* electrochemical methods. The thermal noise (V_{rms}^{th}) is related to resistance (R)

$$V_{rms}^{th} = \sqrt{4k_b TR\Delta f} \tag{3}$$

where k_b is Boltzmann's constant, T is the absolute temperature and Δf is the measuring bandwidth (33). However, this ignores the capacitance of the electrode-solution interface. In an RC circuit, the thermal noise simplifies to

$$V_{rms}^{th} = \sqrt{\frac{k_b T}{C}} \tag{4}$$

More complex equivalent circuits will affect the thermal noise. A metal electrode in contact with an electrolyte can be modelled as a simple RC circuit where the impedance versus frequency is a linear function. Comparison of different electrodes can then be achieved at any frequency. However modification of an electrode with novel materials removes the linear dependence of impedance versus frequency. The choice of measurement frequency then affects any electrode comparisons. Furthermore, when the electrode is placed into tissue, biofouling processes will alter the electrode-tissue interface and may change the equivalent circuit.

An improved correlation of impedance on modified electrodes with electrophysiological response was seen with low frequencies. The low frequency impedance of modified electrodes is dependent on electrode area while the typically reported impedance at 1 kHz is of less utility. Correlation of electrode area with electrophysiological response further confirms the greater relevance of impedance at low frequencies. Therefore a greater theoretical basis of impedance measurements is required to predict electrophysiological performance.

The electrode impedance is a function of the electrical double layer or Helmholtz–Chapman layer formed at the electrode-solution interface. In a simple electrolyte, the electrode impedance behaves as a two-layer system. One layer being the electrical double layer established at the electrode surface, which usually has high impedance. This appears in series with the bulk electrolyte layer, which typically has low impedance. Each layer has a relaxation time (τ) which is a function of their dielectric constant (ε) and conductivity (σ), $\tau = \varepsilon / \sigma = RC$. When charge is applied across these two layers, current will flow. However if the relaxation time of each layer is different, charge accumulation will occur. This is called the Maxwell-Wagner effect (34). In a biological system, cell excitation leads to a change in local ion concentration, charge accumulation at the electrode-tissue interface and subsequent current flow.

In EIS, the electrical-double layer dominates the low frequency response, while the bulk electrolyte dominates the high frequencies. The transition in EIS response between these layers occurs at the Maxwell-Wagner relaxation frequency. Therefore, to measure the electrodes contribution to EIS, frequencies below the Maxwell-Wagner relaxation frequency must be used.

For metal electrodes in simple electrolytes, the Maxwell-Wagner relaxation frequency may be above 1 kHz, and so measurements at this frequency would provide information on the electrical double layer. For systems such as conducting polymer-electrolyte interfaces, the Maxwell-Wagner relaxation frequency will be lower and exhibit higher dispersion; 1 kHz is not a low enough frequency. When the electrode is placed into tissue, protein fouling will affect the electrode-solution interface. The tissue impedance is also far more complex, with a large inhomogeneity in resistivity and permittivity due to variations in cell type and structure and the associated variations in ionic strength and cell membrane capacitance. This prevents measurement of the Maxwell-Wagner relaxation frequency in tissue, and will limit the accuracy in predicting electrophysiological function from *in vitro* electrochemical methods. Nevertheless, the most accurate prediction of electrode performance will be made from low frequency impedance.

Averaging multiple electrode positions reduced biological noise, allowing strong correlations of electrochemical and electrophysiological performance. Residual error may be due to further biological noise caused by the finite number of electrode positions tested. LFPs detect neural activity over a larger region, and the higher correlations seen with LFP than MUA recording implies some biological noise is still present. Some error may also be due to the electrochemical testing (impedance and effective electrode area), which was performed in a simple electrolyte before protein fouling occurred. A more accurate measure of electrode performance may be obtained from an appropriate model solution (ie. artificial cerebrospinal fluid for brain implants and artificial perilymph for cochlear implants).

The neural recording presented here was from acute implantation. This prevents any possible glial cell encapsulation and degradation of the electrode affecting the correlations of electrochemical and electrophysiological performance. During chronic implantation, neural rearrangement, glial encapsulation and electrode degradation can reduce SNR. An ideal device would not suffer any biostability or biocompatibility issues, in which case the chronic performance should approach the acute performance. Before any new devices are assessed for chronic stability, they should be tested via the proposed *in vitro* electrochemical and acute electrophysiological methods. This will reduce costs and numbers of animals used in lengthy experiments with potentially low significance.

Acknowledgements

Funding from the Australian Research Council Centre of Excellence Scheme (Project Numbers CE0561616 and CE140100012) are gratefully acknowledged. The authors thank the Materials Node of Australian National Fabrication Facility (ANFF) and acknowledge use of the facilities.

References

1. Goldman DE. Potential, Impedance, and Rectification in Membranes. J Gen Physiol. 1943;27(1):37–60.
2. Hamill OP, Marty A, Neher E, Sakmann B, Sigworth FJ. Improved patch-clamp techniques for high-resolution current recording from cells and cell-free membrane patches. Pflügers Arch. 1981;391(2):85–100.
3. Nordhausen CT, Maynard EM, Normann RA. Single unit recording capabilities of a 100 microelectrode array. Brain Res. 1996;726(1–2):129–40.
4. Wise KD, Sodagar AM, Ying Y, Gulari MN, Perlin GE, Najafi K. Microelectrodes, Microelectronics, and Implantable Neural Microsystems. Proc IEEE. 2008;96(7):1184–202.
5. Wise KD, Anderson DJ, Hetke JF, Kipke DR, Najafi K. Wireless implantable microsystems: high-density electronic interfaces to the nervous system. Proc IEEE. 2004;92(1):76–97.
6. Wise KD, Angell JB, Starr A. An Integrated-Circuit Approach to Extracellular Microelectrodes. IEEE Trans Biomed Eng. 1970;17(3):238–47.
7. Cook MJ, O'Brien TJ, Berkovic SF, Murphy M, Morokoff A, Fabinyi G, et al. Prediction of seizure likelihood with a long-term, implanted seizure advisory system in patients with drug-resistant epilepsy: a first-in-man study. Lancet Neurol. 2013;12(6):563–571.
8. Kennedy P, Andreasen D, Bartels J, Ehirim P, Mao H, Velliste M, et al. Making the lifetime connection between brain and machine for restoring and enhancing function. In: Jens Schouenborg MG, Nils D, editors. Progress in Brain Research. Elsevier; 2011. p. 1–25.
9. Biran R, Martin DC, Tresco PA. Neuronal cell loss accompanies the brain tissue response to chronically implanted silicon microelectrode arrays. Exp Neurol. 2005;195(1):115–26.
10. Suner S, Fellows MR, Vargas-Irwin C, Nakata GK, Donoghue JP. Reliability of signals from a chronically implanted, silicon-based electrode array in non-human primate primary motor cortex. Neural Syst Rehabil Eng IEEE Trans. 2005;13(4):524–41.
11. Gilletti A, Muthuswamy J. Brain micromotion around implants in the rodent somatosensory cortex. J Neural Eng. 2006;3(3):189.
12. Biran R, Martin DC, Tresco PA. The brain tissue response to implanted silicon microelectrode arrays is increased when the device is tethered to the skull. J Biomed Mater Res Part A. 2007;82A(1):169–78.
13. Lecomte A, Descamps E, Bergaud C. A review on mechanical considerations for chronically-implanted neural probes. J Neural Eng. 2018;15(3):31001.
14. Lee CD, Hara SA, Yu L, Kuo JTW, Kim BJ, Hoang T, et al. Matrigel coatings for Parylene sheath neural probes. J Biomed Mater Res Part B Appl Biomater. 2016;104(2):357–68.
15. Green RA, Matteucci PB, Dodds CWD, Palmer J, Dueck WF, Hassarati RT, et al. Laser patterning of platinum electrodes for safe neurostimulation. J Neural Eng. 2014;11(5):56017.
16. Cui X, Hetke JF, Wiler JA, Anderson DJ, Martin DC. Electrochemical deposition and characterization of conducting polymer polypyrrole/PSS on multichannel neural probes. Sensors Actuators A Phys. 2001;93(1):8–18.
17. Brummer SB, Robblee LS, Hambrecht FT. Criteria for selecting electrodes for electrical stimulation: theoretical and practical considerations. Ann N Y Acad Sci. 1983;405(Cochlear Prostheses An International Symposium):159–71.
18. Apollo N V, Maturana MI, Tong W, Nayagam DAX, Shivdasani MN, Foroughi J, et al. Soft, Flexible Freestanding Neural Stimulation and Recording Electrodes Fabricated from Reduced Graphene Oxide. Adv Funct Mater. 2015;25(23):3551–9.

19. Ward MP, Rajdev P, Ellison C, Irazoqui PP. Toward a comparison of microelectrodes for acute and chronic recordings. Brain Res. 2009;1282:183–200.
20. Shepherd RK, Villalobos J, Burns O, Nayagam DAX. The development of neural stimulators: a review of preclinical safety and efficacy studies. J Neural Eng. 2018;15(4):41004.
21. Martinez J, Pedreira C, Ison MJ, Quian Quiroga R. Realistic simulation of extracellular recordings. J Neurosci Methods. 2009;184(2):285–93.
22. Harris AR, Morgan SJ, Chen J, Kapsa RMI, Wallace GG, Paolini AG. Conducting polymer coated neural recording electrodes. J Neural Eng. 2013;10(1).
23. Harris AR, Morgan SJ, Wallace GG, Paolini AG. A method for systematic electrochemical and electrophysiological evaluation of neural recording electrodes. J Vis Exp. 2014;(85).
24. Paxinos G, Watson C. The rat brain in stereotaxic coordinates. 6th ed. Watson C, editor. Amsterdam: Elsevier; 2007.
25. Kim D-H, Wiler JA, Anderson DJ, Kipke DR, Martin DC. Conducting polymers on hydrogel-coated neural electrode provide sensitive neural recordings in auditory cortex. Acta Biomater. 2010;6(1):57–62.
26. Harris AR, Molino PJ, Kapsa RMI, Clark GM, Paolini AG, Wallace GG. Optical and electrochemical methods for determining the effective area and charge density of conducting polymer modified electrodes for neural stimulation. Anal Chem. 2015;87(1).
27. Lyutov V, Efimov I, Bund A, Tsakova V. Electrochemical polymerization of 3,4-ethylenedioxythiophene in the presence of dodecylsulfate and polysulfonic anions—An acoustic impedance study. Electrochim Acta. 2014;122(0):21–7.
28. Harris AR, Newbold C, Carter P, Cowan R, Wallace GG. Measuring the Effective Area and Charge Density of Platinum Electrodes for Bionic Devices. J Neural Eng. 2018/03/30. 2018;15(4):46015.
29. Harris AR, Molino PJ, Kapsa RMI, Clark GM, Paolini AG, Wallace GG. Correlation of the impedance and effective electrode area of doped PEDOT modified electrodes for brain-machine interfaces. Analyst. 2015;140(9).
30. Barsan MM, Pinto EM, Florescu M, Brett CMA. Development and characterization of a new conducting carbon composite electrode. Anal Chim Acta. 2009;635(1):71–8.
31. Harris AR, Paolini AG, Wallace GG. Effective Area and Charge Density of Iridium Oxide Neural Electrodes. Electrochim Acta. 2017;230.
32. Downey JE, Schwed N, Chase SM, Schwartz AB, Collinger JL. Intracortical recording stability in human brain–computer interface users. J Neural Eng. 2018;15(4):46016.
33. Baranauskas G, Maggiolini E, Castagnola E, Ansaldo A, Mazzoni A, Angotzi GN, et al. Carbon nanotube composite coating of neural microelectrodes preferentially improves the multiunit signal-to-noise ratio. J Neural Eng. 2011;8(6):66013.
34. Iwamoto M. Maxwell–Wagner Effect BT - Encyclopedia of Nanotechnology. In: Bhushan B, editor. Dordrecht: Springer Netherlands; 2014. p. 1–13.

Table 1. Average, standard deviation and coefficient of variation of outside stimulation RMS potential, signal-to-noise ratio and mean during stimulation spike count.

Polymer coating	Outside stimulation RMS potential (μV)				Signal-to-noise ratio			Mean during stimulation spike count		
	Ave	SD	CV	Max	Ave	SD	CV	Ave	SD	CV
15s PEDOT-PSS	10.2	0.7	0.07	6.18	3.86	0.16	0.04	20.2	1.3	0.06
30s PEDOT-PSS	11.5	2.2	0.19	6.48	3.63	0.87	0.24	20.5	1.9	0.09
45s PEDOT-PSS	10.5	1.7	0.16	5.57	3.62	0.60	0.16	20.3	1.6	0.08
60s PEDOT-PSS	12.0	2.6	0.22	4.97	3.02	0.44	0.15	18.0	2.4	0.13
45s PEDOT-pTs	15.4	6.0	0.39	4.24	2.89	0.64	0.22	19.2	3.6	0.19
Uncoated	17.7	9.8	0.55	2.20	1.83	0.33	0.18	9.6	4.0	0.42
15s PEDOT-DBSA	11.2	1.8	0.16	4.04	3.21	0.95	0.30	18.2	3.3	0.18
30s PEDOT-DBSA	12.1	2.5	0.20	4.73	3.41	0.42	0.12	20.3	2.8	0.14
45s PEDOT-DBSA	9.9	0.1	0.08	4.94	3.65	0.15	0.04	21.0	1.1	0.05
60s PEDOT-DBSA	11.6	3.1	0.27	3.90	3.18	1.00	0.32	19.1	1.6	0.08
45s PEDOT-pTs	17.6	5.3	0.30	3.02	2.42	0.95	0.39	17.8	5.2	0.29
Uncoated	21.0	10.9	0.52	2.21	1.67	0.25	0.15	7.2	2.7	0.37

Figures

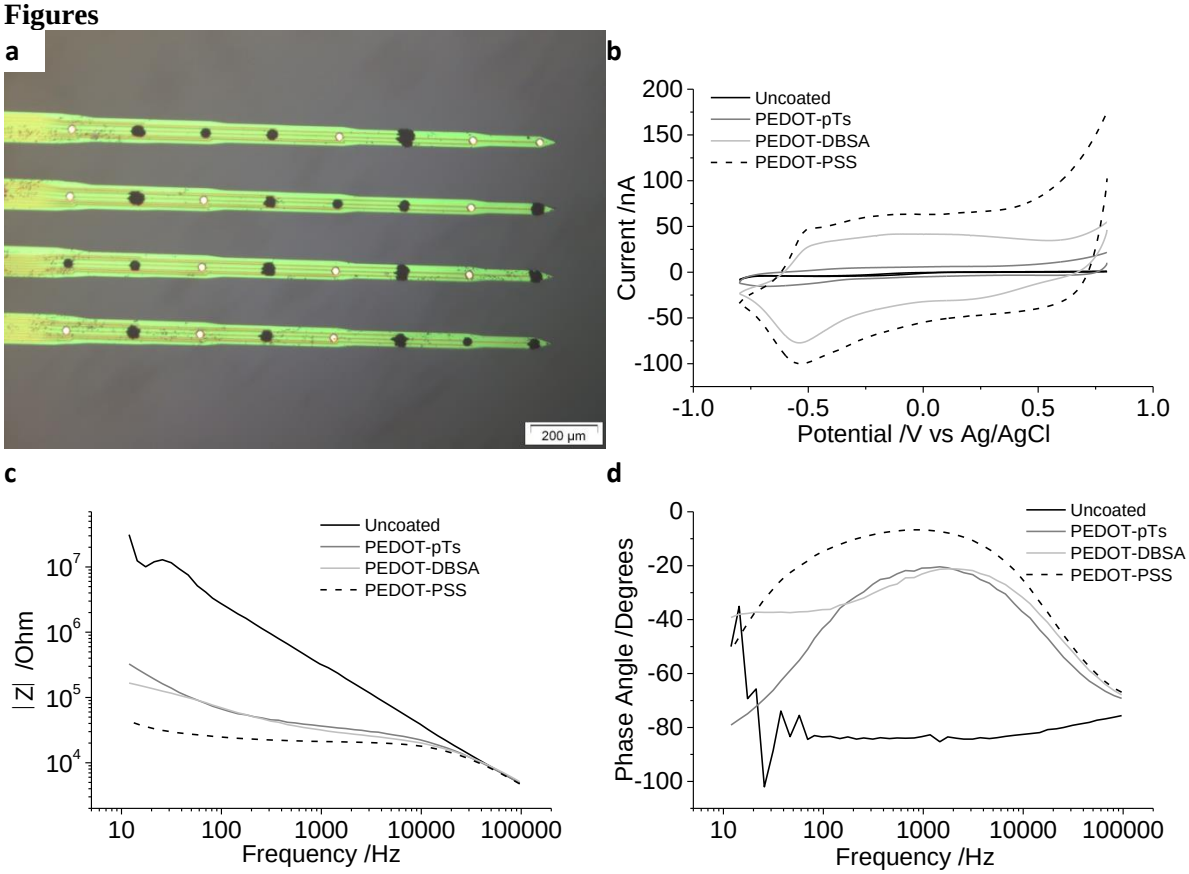

Figure 1. (a) Visible light microscopy of a PEDOT-DBSA modified probe. (b) Typical cyclic voltammetry and (c-d) electrochemical impedance spectroscopy in 0.3 M Na_2HPO_4 at 100 mV s^{-1} of an uncoated electrode; and electrodes coated at 45 s deposition of PEDOT-pTs, PEDOT-DBSA or PEDOT-PSS.

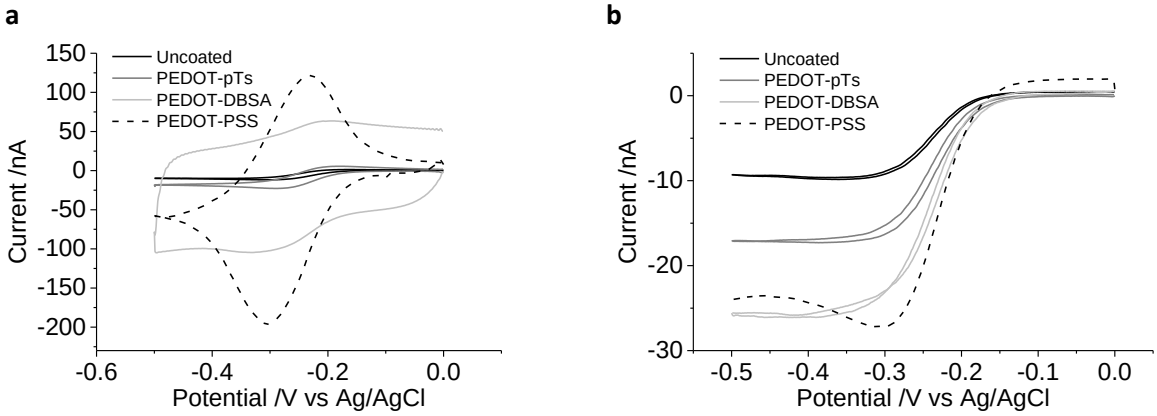

Figure 2. Typical cyclic voltammetry of 5 mM $Ru(NH_3)_6^{3+}$ in 0.3 M Na_2HPO_4 on uncoated electrode; and electrodes coated at 45 s deposition of PEDOT-pTs, PEDOT-DBSA or PEDOT-PSS. (a) At 200 mV s^{-1}, all background subtracted except for PEDOT-DBSA. (b) At 10 mV s^{-1}, all background subtracted, only the reductive scan of PEDOT-PSS is shown.

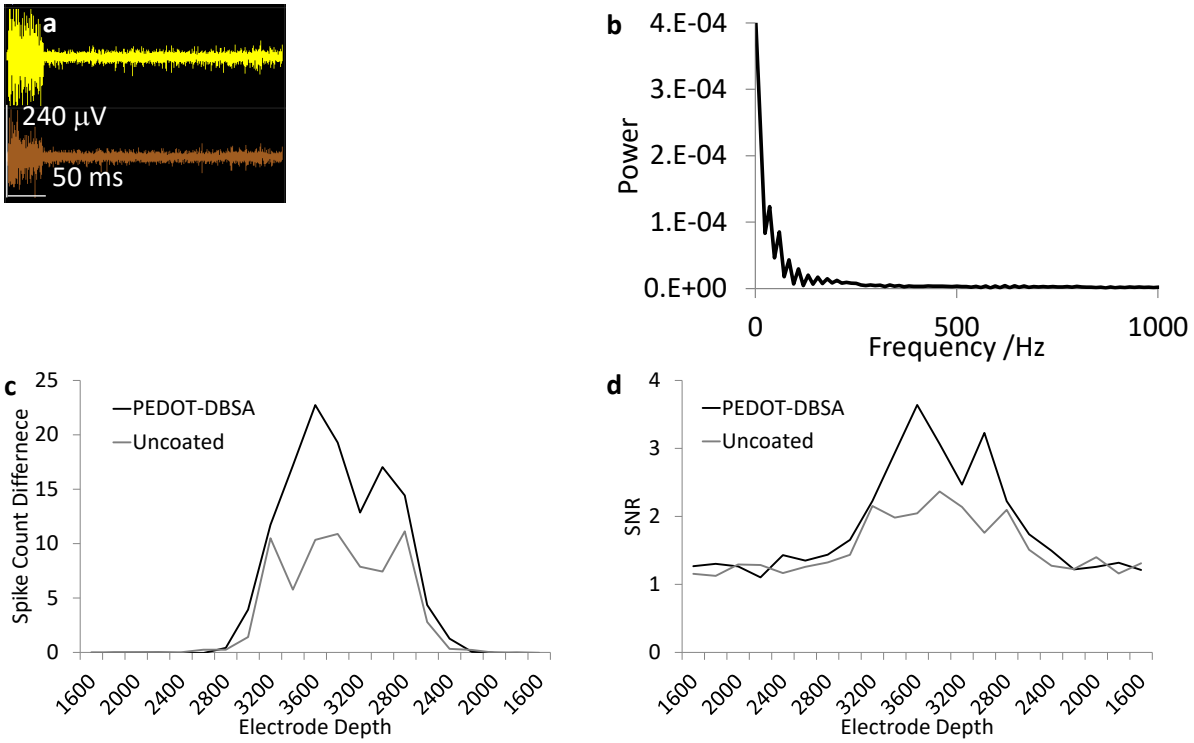

Figure 3. (a) Typical streaming data of a 50 ms white noise pulse of a coated (yellow) and uncoated (brown) electrode. (b) Power spectrum of 300 repetitions of white noise pulses. (c) Spike count difference and (d) SNR of a PEDOT-DBSA and an uncoated electrode during insertion and withdrawal into the IC.

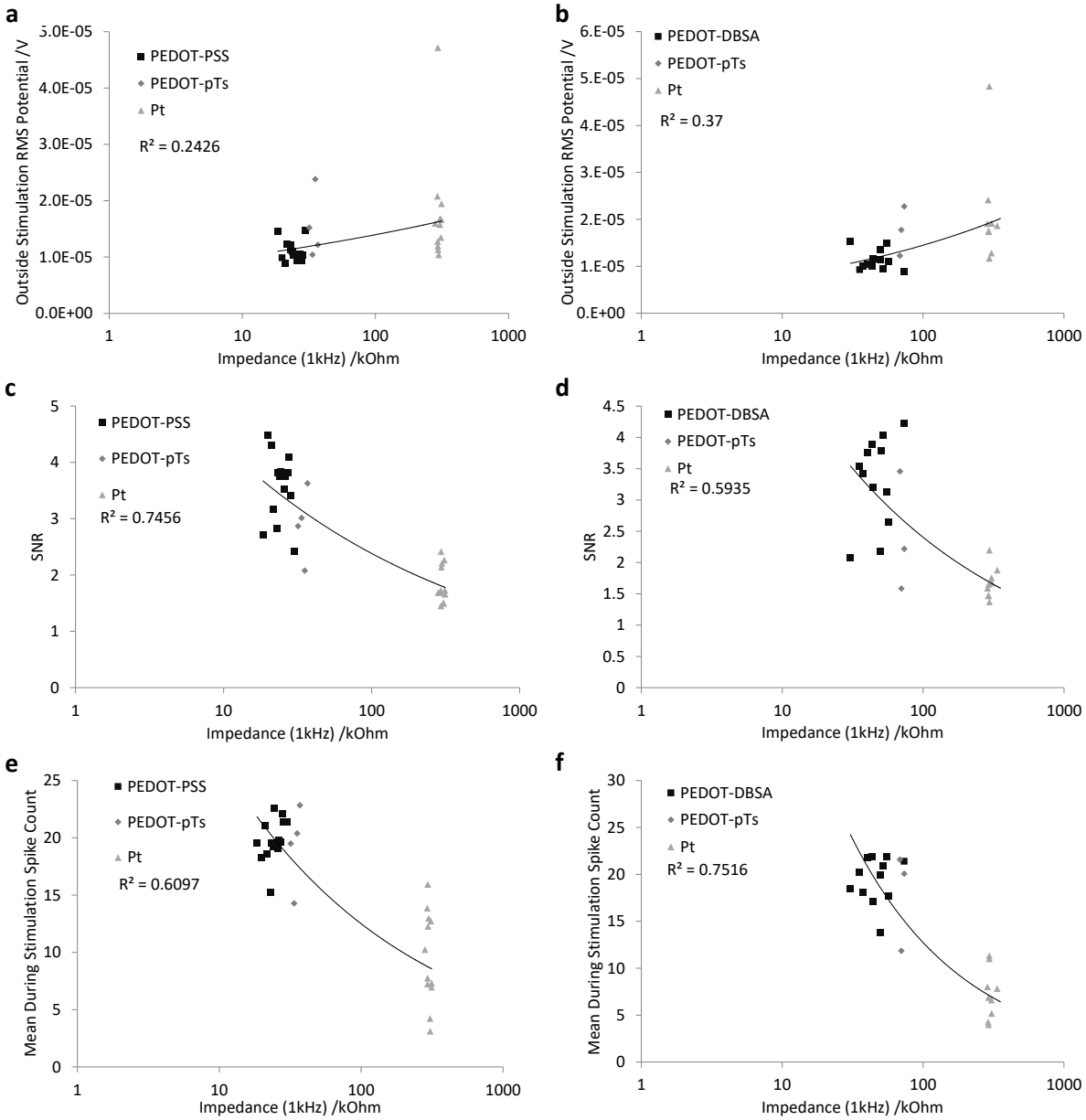

Figure 4: Impedance at 1 kHz at (a, c, e) PEDOT-PSS and (b, d, f) PEDOT-DBSA modified electrodes versus (a-b) RMS_{bkgd}, (c-d) SNR and (e-f) mean during stimulation spike count. The fitted trendlines are power curves.

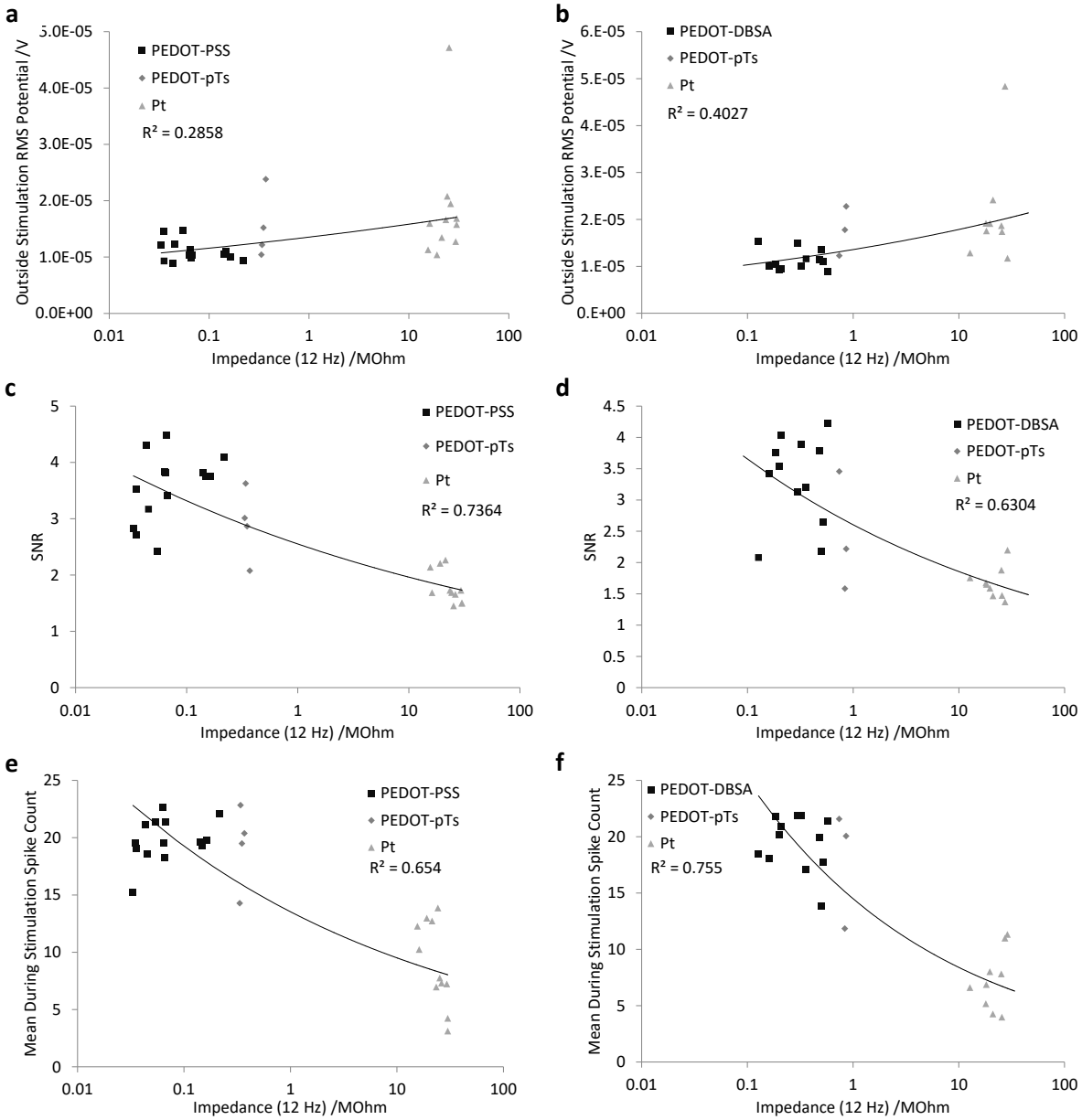

Figure 5: Impedance at 12 Hz at (a, c, e) PEDOT-PSS and (b, d, f) PEDOT-DBSA modified electrodes versus (a-b) RMS_{bkgd}, (c-d) SNR and (e-f) mean during stimulation spike count. The fitted trendlines are power curves.

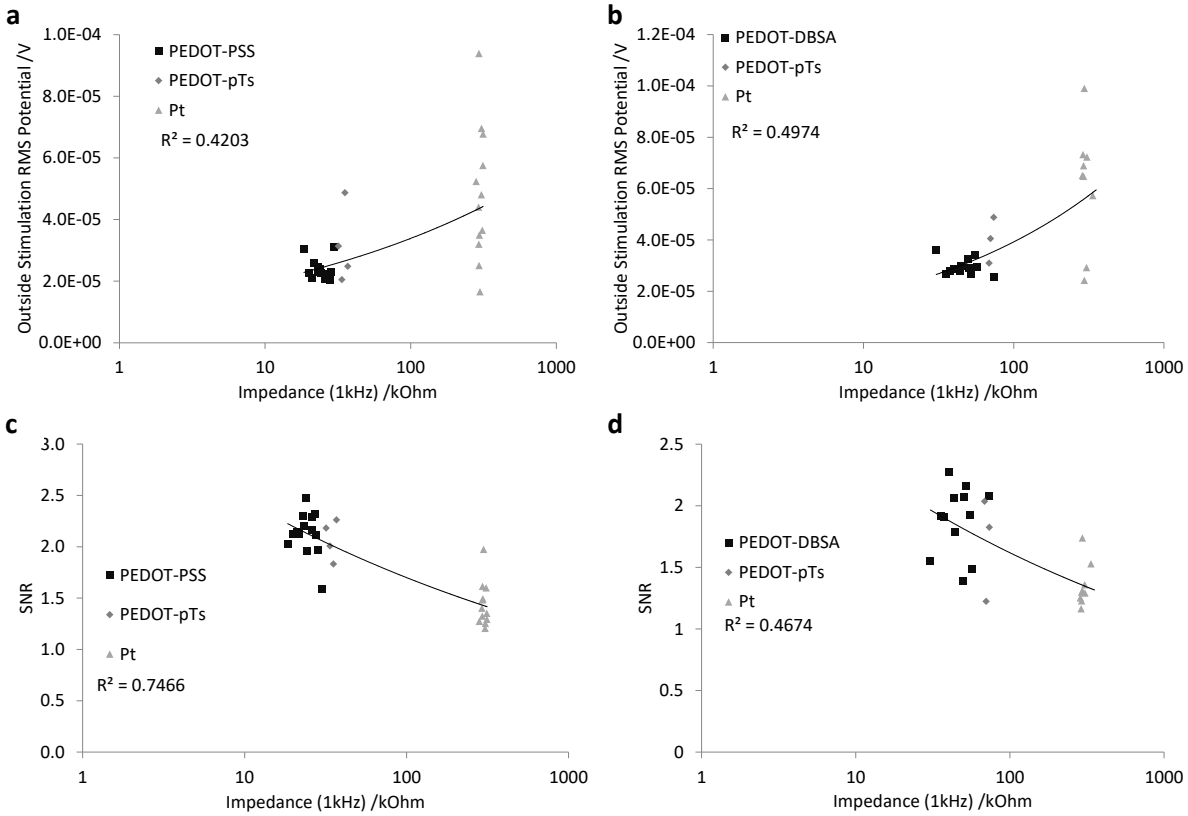

Figure 6: Impedance at 1 kHz at (a, c, e) PEDOT-PSS and (b, d, f) PEDOT-DBSA modified electrodes versus local field potential (a-b) RMS_{bkgd} and (c-d) SNR. The fitted trendlines are power curves.

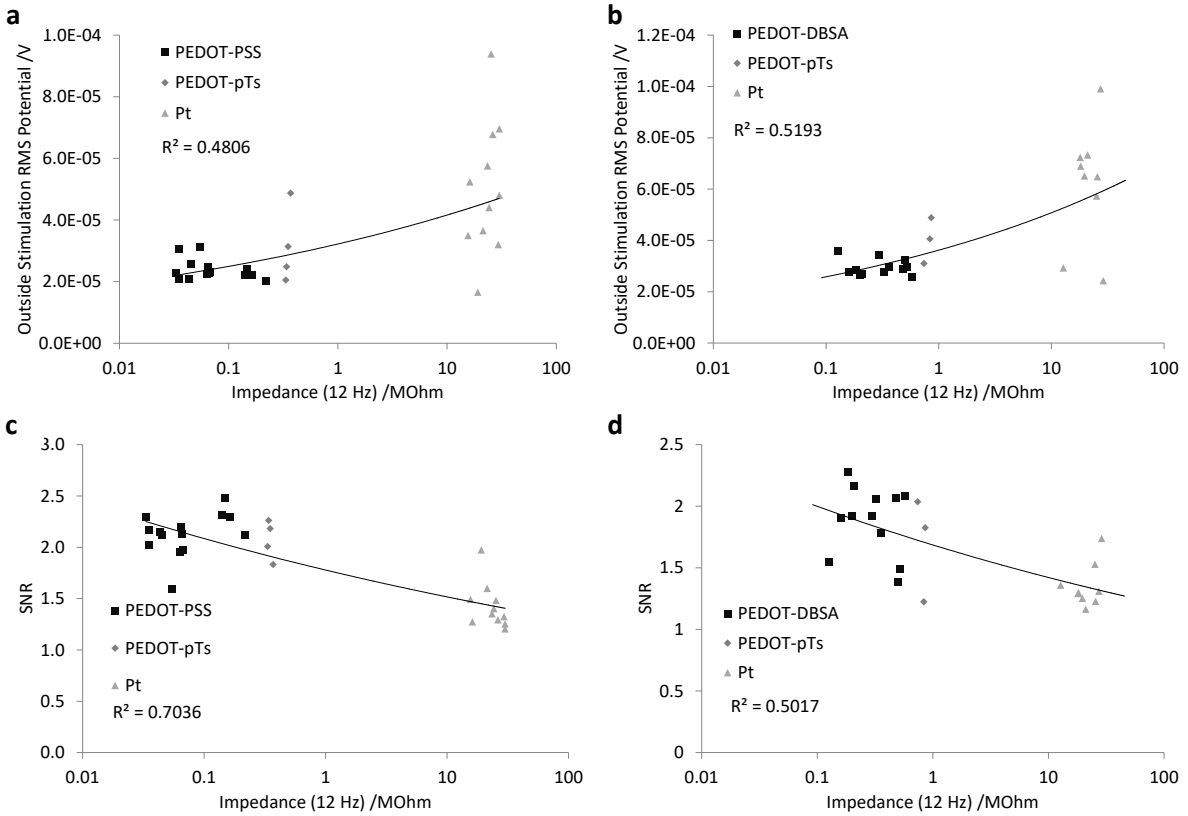

Figure 7: Impedance at 12 Hz at (a, c, e) PEDOT-PSS and (b, d, f) PEDOT-DBSA modified electrodes versus local field potential (a-b) RMS_{bkgd} and (c-d) SNR. The fitted trendlines are power curves.